eNut: A Sensing System to Measure the Acquisition of Foraging Proficiency in Wild Tree Squirrels

Mihir S. Chauhan, Avikam Chauhan, *Member, IEEE*, Myriam Bayen, Fangyu Wu, Fahd A. Althukair, Michael T. Kaiser, and Lucia F. Jacobs

***Abstract*—We present a three-part sensing system to measure the acquisition of foraging proficiency in wild tree squirrels. The first component is the *eNut*: a 3-D printed enclosure in the size and shape of a large food item, such as a walnut. The *eNut* contains an inertial measurement unit (IMU), consisting of an accelerometer and a gyroscope, along with a capsule containing a food reward (e.g., chopped nuts), motivating the squirrel to manipulate the *eNut* to open the reward capsule. The second component is a radio frequency identification (RFID) gate that can detect the presence of a known individual. The reader generates time-stamped labels for the analysis of simultaneous video recordings of the squirrel movements. Finally, the third component is a data collection pipeline, which aggregates the sensor data in a cloud backend server. The design process culminated in a fully functional prototype system tested under three field conditions: two outdoor sites used for juvenile squirrel rehabilitation and a third site with free-ranging adult squirrels. The accuracy of the collected data is assessed by leveraging laboratory settings in which acceleration and rotation were checked against reference values produced by a testing infrastructure, custom-built for this application. Finally, we present an inventory of food item manipulation movements (rotation and shaking) that are identified and quantified with the *eNut* system. This system allows a level of granular analyses of foraging decisions that was not feasible with prior technology, which would have important translational value in paradigms of animal behavior and wildlife rehabilitation.**

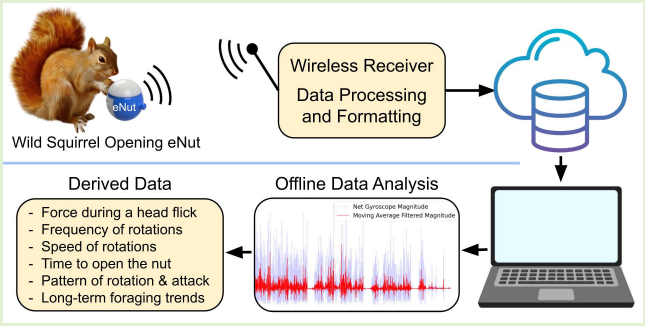

***Index Terms*— Accelerometer, animal behavior, biologging, foraging decision, gyroscope, inertial measurement unit (IMU), radio frequency identification (RFID), sensing system, wildlife rehabilitation.**

I. Introduction

ADVANCES in sensor technology have greatly improved the study of animal behavior, allowing for observations of previously unobservable behaviors. Dramatic examples, using a "black box" methodology, allow biologists to create a daily diary of behaviors, even in previously inaccessible species such as deep-diving penguins [1]. With the continued miniaturization of sensors, biologists are now able to track animals from insects to cheetahs, across enormous scales of time and space. Furthermore, the employment of machine learning leads the field to new conceptual heights, with the ability to analyze the big data of the new biologging sensors [2]. The bulky, power-hungry telemetry tags of prior decades limited research to species of a minimum body size and to studies whose duration was constrained by battery size and weight [3].Modern sensing systems have allowed for new types of animal behavior monitoring and data collection, such as the eating and drinking behaviors of cattle on farms [4], [5], [6]. Wearable inertial measurement units (IMUs) have extended to uses such as tracking multibody dynamics of cheetahs [7] as well as using machine learning models for classifying high-level animal behaviors (sitting, walking, running, etc.) [8] and [6]. Sensors such as radio frequency identification (RFID) tags [9] and triaxial accelerometers [10] are now widely used in wildlife studies, and have expanded the scope of research to include physiological and cognitive processes, as well as processes that would be biased by the presence of the human observer [11].

Manuscript received 21 June 2024; accepted 13 July 2024. Date of publication 23 August 2024; date of current version 2 October 2024. This work was supported by the Army Research Office Multidisciplinary University Research Initiatives (MURI) Program through Lucia Jacobs under Grant 574723. The associate editor coordinating the review of this article and approving it for publication was Dr. Abhishek Kumar Jha. *(Corresponding author: Avikam Chauhan.)*

This work involved human subjects or animals in its research. Approval of all ethical and experimental procedures and protocols was granted by the University of California at Berkeley Animal Care and Use Committee.

The authors are with the Departments of EECS and Psychology, University of California at Berkeley, Berkeley, CA 94709 USA (e-mail: mihir_chauhan@icloud.com; avikam.chauhan@berkeley.edu; myriam.bayen.2008@gmail.com; fangyuwu@berkeley.edu; falthukair@berkeley.edu; mike.kaiser@berkeley.edu; jacobs@berkeley.edu).

Digital Object Identifier 10.1109/JSEN.2024.3435834

For instance, accelerometer-based sensing systems have been used to monitor the activities (e.g., walking, running, eating, and drinking) of large free-roaming animals [12]. Similar accelerometer-based sensing devices, paired with a network of Zigbee receiver nodes, have also been shown to be useful for monitoring the activity levels of wild monkeys [13]. These devices have also been used to record the differences in movement patterns of animals with neurological defects like multiple sclerosis [14]. Multisensor IoT devices, paired with a data pipeline using Arduino microcontrollers and a cloud backend, can also be used to monitor the vitals (e.g., heart rate, oxygen levels, temperature, and movement) of household animals [15]. Although the real-world accuracy of such sensors, primarily accelerometers and gyroscopes, are often inconsistent [16] due to instability of random bias [17], there have been several analyses for effective methods of resolving changes in position and orientation with filters (moving average, alpha–beta, and Kalman) to reduce noise and improve estimation accuracies [17], [18]. Such a capacity to measure behavior unobtrusively in remote settings has powerful implications for progress in the study and conservation of threatened and endangered species [2].

A. Context of the Work

Our goal in the present study is to employ these established sensor technologies in a novel application: instrumenting an electronic food item in a closed foraging system, where the forager's identity and location are registered by RFID and video records. To our knowledge, this is the first study where instead of instrumenting the forager, we are instrumenting the food item. The rationale for this design is derived from our larger research goal, which is to study the acquisition of survival skills in captive juvenile squirrels being held in wildlife rehabilitation centers.

New research in conservation biology has demonstrated the importance of scaffolded learning—termed "headstarting"—during development for endangered species [19]. Vertebrate species with complex life history strategies, such as tree squirrels, face steep challenges to learn to forage and seek refuge, while at the same time, escaping predation. Under natural conditions, juvenile tree squirrels show extreme rates of mortality during their period of development, as close to 75% of squirrels die [20]. In a songbird species (yellow-eyed Junco), juvenile mortality results from inadequate learning experiences, which leads to starvation from poor foraging skills and predation from poor escape skills [21], [22]. Learning is important for locomotion: wild fox squirrels show flexible "parkour" motor learning while leaping gaps between artificial branches in an experimental apparatus [23].

While juvenile squirrels have an innate propensity to gnaw on items exuding food odors, this is shaped via experience and learning [24], [25], which includes skills gained from observing experienced adults [26]. The juvenile tree squirrel raised in captivity thus faces the important challenge of learning to manipulate and open the hard nuts that its future survival depends on.

Both species of tree squirrels in our study, the Eastern Gray Squirrel (*Sciurus carolinensis*) and the Fox Squirrel (*Sciurus niger*), are specialized scatter hoarders, creating food caches with a single deposit. In contrast, larder hoarding squirrel species use multiple deposits to create large middens. But scatter hoarders rely on spatial memory to efficiently retrieve their scattered caches during periods of scarcity [27]. Because each seed or nut is cached separately, the scatter hoarder faces a complicated decision tree: first, whether to eat or cache, decided by opportunity costs at that moment [28], [29], [30], and second, how much time and energy to invest in the manufacture of the cache [31].

According to the inherent value of the food item, squirrels strategically invest their efforts to reduce the risk of cache pilferage. Some of the investments that are proportionate to the value of the item are how far the item is carried, the nearest-neighbor distance to the next cache and spatial chunking, or placing similar items in the same area, a tactic which reduces the cognitive load of recall [32], [33].

Thus, it is critical for scatter hoarding species to precisely assess the characteristics of a food item. This has only been studied in one species of squirrel [31] and three species of birds. Jays and nutcrackers in the crow family (Corvidae) assess an item by clacking it in their beak, where the sound of the seed hitting the beak in this way is apparently diagnostic of the seed's quality [34], [35], [36].

Two nut assessment movements have been identified in tree squirrels [31]. These are: the paw manipulation, where the nut is rotated by the paws while being held in the mouth, and the head flick, where the squirrel grasps the nut firmly in its mouth and flicks its head from side to side. The head flick is characteristic of these two obligate scatter hoarding species, the subjects of the present study.

B. Contributions of the Article

This article presents a high-fidelity, multimodal hardware/software sensing system that enables quantitative animal psychology research in a variety of environments. Specifically, this system enables scientists to study how squirrels approach, interact with, and learn about their food. This is, to our knowledge, the first design of a food item instrumented with sensors to quantify animal foraging skills—in this case, a squirrel's ability to open a nut. The food-mounted sensor is embedded inside a 3-D printed nut, the *eNut*, which is itself integrated into a system of remote RFID readers and video cameras that record the identity and behavioral context of the foraging bout with the sensor-equipped food object, the *eNut*. The *eNut* sensors are capable of detecting movements (force, rotation, and acceleration) previously documented in squirrels making assessment decisions about nuts. Our system can collect data through three different pipelines, incorporating different devices for different experimental settings, ranging from caged squirrels to wild squirrels in open areas. These pipelines include a smartphone app, laptop app, and an Arduino receiver (for cage settings), all of which pair with the *eNut* for wireless data transmission. The data is recorded on-device and then aggregated on a cloud backend server. Finally, with our custom data processing software, we are able to extract a variety of metrics for each squirrel interaction, including the following: band of actuation (in frequency domain),

time taken to open the *eNut*, total number of rotations, distribution of rotation speeds, and distribution of shaking forces.

The article is structured as follows: In Section II, we outline the several design constraints and desirable metrics that can be extracted from collected data. In Section III, the *eNut* system is presented, including the physical nut enclosure, the data pipelines that have been utilized to collect data in several experiment settings, and methods of time-tagging data for postexperiment analysis. This section also includes the RFID and video camera system to perform longitudinal studies of individual squirrel interactions with the *eNut*. Section IV discusses the three sites of squirrels for which the procedure for conducting experiments is outlined. In order to ensure the field work accuracy of data and its analysis procedures, in Section V we discuss the several experiments we conducted of accelerometer and gyroscope motion in controlled settings while outlining extractable metrics (through Fourier analysis, net acceleration graphs, etc.) Section VI presents data collected in our squirrel cage settings and the many metrics that have been successfully extracted. Finally, Section VII summarizes the contributions of this article while documenting several improvements and methods of performing large-scale studies and further analyzing squirrel foraging behaviors.

II. Problem Statement

A. Squirrel Monitoring System

Prior studies of this fundamental problem in the life of the juvenile squirrel—how to assess the value of a food item to inform its cache investment decision—have had to rely only on analysis of direct observation and video records. Here, we harness the power of sensor technologies to precisely measure the assessment behaviors (rotation and head flicks) employed by known individual squirrels in a captive setting, where the squirrel's identity and location is derived from simultaneous records from video- and custom-designed RFID readers. In addition to naive captive juveniles, learning to handle nuts for the first time, we measure the same movements in wild adult squirrels, with extensive foraging experience but also naive to the instrumented food item (*eNut*). Prior studies of this behavior in wild adult squirrels identify three key parameters in the squirrel's assessment decision that can be manipulated experimentally: the mass, volume, and species of food item. This is the parametric space, within which we will explore the decision-making processes of the squirrel in response to the qualities of the food item it encounters. Our sensing system generates the data used to infer the behavior of the squirrel, measured 24/7 in a remote setting, and calibrated with a time-stamping RFID gate and simultaneous video records. A modular data collection pipeline tags the identity of the squirrel and the time of entry to the zone of interest to interact with the *eNut*. The pipeline records key handling parameters: the force exerted during a head flick, the number, frequency, and speed of rotations, the time invested in opening the nut, and the overall pattern of rotation and attack (gnawing).

B. System Requirements

In order to provide the required data, the system proposed needs to provide the following quantities.

1) Time-tagged video, for further animal behavioral studies.
2) Acceleration and rotation of the *eNut* as raw data for the study.

With this, and as is illustrated in the rest of this work, the developed system enables us to record time-series data, from which numerous useful animal behavioral characteristics can be extracted, such as engagement time (the amount of time a squirrel spends working at the *eNut*), opening time, amount of rotation before opening, amount of shaking during the process, and frequencies at which the squirrel operates.

III. System Design

This section describes the design of the proposed squirrel activity monitoring system. The system includes three components, described below: 1) the *eNut*, which we use to measure the squirrel activity; 2) the RFID gate, which we use to time-tag the activities of the squirrel (using an RFID chip we inject into the squirrel) on the video collected by the cameras of the system; and 3) and finally the data integration pipeline, used downstream of the system to aggregate the measurements.

A. Sensor (eNut)

1) 3-D Printed Enclosure: The *eNut* was designed to mimic the natural form of large tree seeds that these species have co-evolved with as seed consumers and dispersers [37]. Given the constraints of hardware size and form-factor, the 3-D printed enclosure is similar to a large English walnut. There are three key components of the design.

1) A bottom section constructed in two pieces. It contains an armored internal cavity enclosing the *Puck.js* and up to two quarters (USD 25 cent coin) for additional weight variation. The two pieces are attached together with screws. The entire bottom section protects the electronic components from the squirrel gnawing. This design also facilitates the removal and replacement of the printed circuit board (PCB) and sensing hardware.
2) A top section in the form of a hollow capsule on one end containing a food reward (e.g., chopped walnuts and peanut butter) on the top of the *eNut*. The top surface of the capsule is perforated, so that the food odor can be detected. The squirrel must thus crack open the capsule to consume the contents, which mimics the opening of a hard nut such as a walnut.
3) A projection acting as a stem on the capsule, facilitating the natural behaviors of grasping, head flicking, and carrying a nut to a different location, either to consume or cache it.

Fig. 1 depicts the final *eNut* design, consisting of three 3-D printed components. The two components that make up the bottom half of the *eNut* contain a cavity where the *Puck.js* is installed, along with space for up to two quarters (for additional weight variation). The lid is secured on top of the *eNut* with a nontoxic glue.

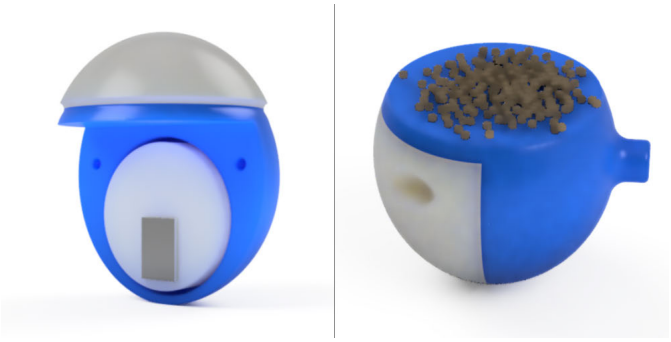

Fig. 1. **Left:** final *eNut* design showing the *Puck.js* PCB inside one half with top cap on. **Right:** final *eNut* design showing enclosed bottom half with walnut crumbs on top, cap not shown.

2) Sensing Hardware: We chose the *Puck.js* for the *eNut* hardware because it provides a compact, low-power Bluetooth-enabled multisensor that fits our design constraints. This type of sensor has been used for applications such as fall-prevention systems for older adults [38] and function status measurements for adults with Alzheimer's [39]. Some of the sensors in this package include the following: accelerometer, gyroscope, magnetometer, light, and temperature. The firmware runs a custom implementation of the *Espruino* JavaScript interpreter, allowing software to be written in JavaScript. The *Espruino* firmware was modified to set the sensors to run in their high performance mode (with higher output data rates) as well as enable hardware I^2C instead of the default software polling method. The *Puck.js* is powered by a user-replaceable CR2032 battery, which made it convenient both in terms of physical size and in terms of operating the device. Using our custom firmware and JavaScript software, we were able to stream six-axis IMU (accelerometer and gyroscope) data over Bluetooth Low Energy (BLE) at up to 250 Hz. The physical PCB is a 29 mm circle, approximately 8.5 mm thick, which fits well within the design constraints of the *eNut*.

3) Data Pipelines: We initially developed the first *eNut* sensor data pipeline to utilize our existing hardware setup designed for the RFID gate (i.e., an *Arduino Uno* board). To interface the *Arduino Uno* with the *Puck.js* (a BLE-enabled device), we added the *Arduino Nano BLE* board. Our software on the *Arduino Nano BLE* receives sensor data at up to 20 Hz over BLE from the Puck.js, and transmits the recieved sensor data to the *Arduino Uno* over a serial I^2C channel. This is then handled by firmware on the *Arduino Uno*, which stores the data in *.csv* format on an SD card, and periodically uploads this to a Firebase database on Google Cloud (using the Firebase library for *Arduino*). Then, we can access the data for visualization and analysis with our Python scripts using HTTP requests to the database.

In order to accommodate a higher data throughput in this system, we decided to explore alternative pipelines that allow us to collect higher frequency data. We developed a mobile app for iOS that allowed for live data visualizations, faster data collection, and easy portability/sharing of data. This platform allowed us to collect data at up to 50 Hz, and we tested data collection for a few experiments using this pipeline.

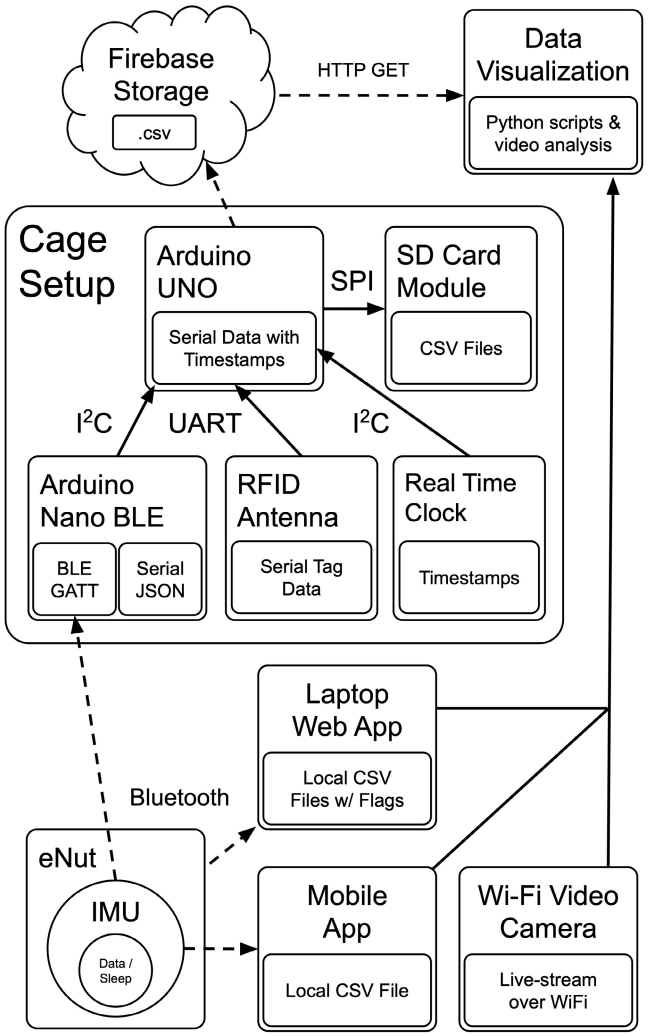

Fig. 2. Three paths for accelerometer and gyroscope data to be streamed from the *eNut*. The path used depends on the type of data collection: asynchronous, in-cage (using the *Cage Setup*), or synchronous (using the mobile app or laptop web app).

However, to achieve the maximum possible data throughput with this sensing hardware, we developed a web app for macOS/Windows that (using BLE serial) can receive data at up to 250 Hz. This is the most performant pipeline that we developed, and it is what we used for the majority of our experiments. Fig. 2 depicts various pipelines we developed, as well as the associated hardware components used and the communication protocols employed.

4) Data Collection: To collect data, we pair the *Puck.js* with the preferred data collection node (e.g., *Arduino Nano BLE*, smartphone, or laptop), and install it inside the *eNut*. Then, we can remotely start/stop the streaming of data through the respective software. We also utilized on-device motion detection algorithms to preserve battery life and avoid streaming sensor data when the device is at a standstill (i.e., the squirrel is not interacting with the *eNut*).

5) Time-Tags: Our data collection software has a tagging feature, which allows us to manually log timestamps when squirrels exhibit useful/relevant behaviors. This serves to assist with the downstream data analysis. The tags are used to mark

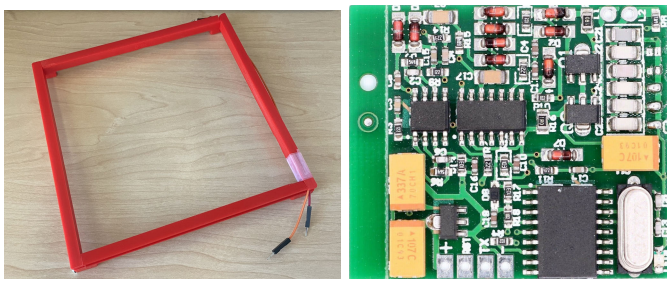

Fig. 3. **Left:** final version of 3-D printed RFID antenna frame. **Right:** front view of the RFID reader PCB (approximate size: 35 mm by 36 mm).

important times during the *eNut* opening (e.g., started/stopped moving around the cage, started/stopped rotating the *eNut*, started/stopped shaking the *eNut*, opened the *eNut*, dropped the *eNut*, etc.). Once the *eNut* is opened, the data collection is stopped, and both the six-axis IMU data and a separate file with all of the tagged timestamps are saved. Afterward, we record event descriptions for each tag and save it with the corresponding flag file. When processing the videos and sensor data, we can synchronize the streams using their respective timestamp information. Then, using the tagged timestamps, we can segment the data based on the squirrel's actions/behavior.

B. Squirrel Monitoring System (RFID + Video Camera)

1) Squirrel ID and Time-Tagging System: The full system was designed to operate continuously and monitor multiple squirrels simultaneously.[1] Thus, we needed a component of the system to produce the following two attributes for the data.

1) *Squirrel Identification:* We need an automated way to detect which squirrel is handling the *eNut*, so we can perform longitudinal studies on individual squirrels.
2) *Time-Tagging:* In order to process squirrel activity video data more efficiently, we need to record timestamps corresponding to their activities. This is achieved through the design and deployment of an *RFID gate*, which triggers a timestamp log each time a squirrel (with a unique RFID tag embedded) goes through the gate to get the *eNut*. Most animals found orphaned and saved by animal shelters in California are chipped for further monitoring purposes before they are released in nature. In the present case, we worked with two shelter organizations and provided them with RFID tags that are compatible with our system; the RFID tags were injected into the squirrels by animal shelter staff.

2) RFID Gate: The RFID gate was designed and deployed in Site 2, so we could perform longitudinal studies of individual squirrels. It consists of a 3-D printed frame that the squirrels have to pass through to grab the *eNut*. The 3-D printed frame is designed to enclose an RFID antenna coil, which is used to detect the RFID tag (preinjected into the squirrel) when the squirrel goes through the gate.

The RFID reader is an off-the-shelf system called *134.2 K AGV RFID Long Range Animal Tag Embed Reader Module*. The reader is capable of reading tags at a frequency of 134.2 kHz. The front of the PCB is shown in Fig. 3, and its dimensions are approximately 35 mm by 36 mm, with the accompanying antenna measuring at 97 mm by 97 mm. The supply voltage range is 5–9 V and at 9 V, the working current is around 120 mA. The inductance of the antenna is about 580 μH.

We use an emulated serial communication on an *Arduino Uno* to interface with the RFID reader. The following pseudocode snippet, derived from an online forum post [40], describes how to receive and decode the payload sent by the RFID tag.

Algorithm 1 RFID Reader Pseudocode

```
1. import necessary libraries
2. set up global variables
procedure SETUP
    1. initialize serial port for RFID reader
    2. initialize real-time clock
    3. initialize file system interface
    4. connect to local Wi-Fi network
end procedure
procedure LOOP
    while true do
        poll RFID reader for new tags
        if new tag detected then
            1. decode tag ID using bitwise operations
            2. save event log in.csv format to SD card
            3. queue event for logging on ThingSpeak
        end if
    end while
end procedure
```

Because each RFID tag has a unique numerical identifier, we can identify the squirrels as they pass through the RFID gate.

3) Iterative Design Process: The design of RFID systems took two iterations. In the final iteration, we referenced an *Arduino*-based RFID reader, developed as part of the University of Oklahoma Biologging Initiative [41]. The *Arduino*-based RFID reader is equipped with an SD card module, a real-time clock, and an embedded EM4095 RFID reader-integrated circuit. The EM4095 circuit by default supports reading RFID tags at 125 kHz, which was different from our 134.2 kHz animal tags. The existing reader, however, worked with 134.2 kHz tags, performed reliably, and is easy to use with an *Arduino Uno*. The amount of code required is minimal and is readily available from *Arduino* forums.

C. Downstream Data Integration

To combine the two systems used above, we integrated the RFID tag detection with the *eNut* data streaming pipeline, thus simplifying the hardware setup. This allows for a compact solution for centralized data logging and monitoring, and the data can be uploaded to a backend webserver for analysis. However, there were some challenges with implementing this on a single-threaded *Arduino Uno* (where time-slicing led to slower data rates), so we propose the future development of custom hardware for both the *eNut* and centralized collection system to avoid this problem.

[1] Each of the squirrels carries a different RFID tag with a unique ID.

Fig. 4. **Left:** site 1 cage (Piedmont, CA). **Middle:** Site 2 cage (Novato, CA). **Right:** site 3 (UC Berkeley Campus).

IV. Data Collection Procedures

The components of the system were tested in three different sites depicted in Fig. 4. Two sites are rewilding cages: Site 1, located in Piedmont, CA, and Site 2, located in Novato, CA. The specific components of the system tested in the three sites as well as the squirrel demographics used are described next.

A. Rewilding Site 1: Captive Juvenile Fox Squirrels

1) Study Animals: Six Fox Squirrels (two females and four males), orphaned in three sites (Alameda County, CA), were rescued by wildlife rehabilitators in March 2023. These squirrels were then bottle fed in captivity, with a slow introduction to solid foods and nuts in the shell. By the age of ten weeks, all squirrels were opening and eating nuts, and by the age of 12–14 weeks, all squirrels were transferred to Site 1, an outdoor rewilding cage (Piedmont, CA). Here, they were habituated to outdoor conditions, eating a diet of fruit, nuts, and vegetables for an additional four weeks. At the age of 19–21 weeks, the group of squirrels was presented with a series of baited *eNuts*. The *eNut* exposure continued for 1–2 weeks, after which the squirrels were released into natural habitat.

2) Procedure: The original food reward for this group was chopped walnuts. The squirrels, however, did not attempt to open these *eNuts*. After being given more exposure to walnuts in the diet, the squirrels began to pick up the *eNut* and attempt to rotate and open it. Such efforts were not sustained and no squirrel succeeded in opening the *eNut*. A new method was tried: a thin layer of peanut butter was applied to the top capsule, covering the perforations, with several pieces of peanut kernel placed on top of this layer. This change in protocol succeeded in attracting the attention and efforts of the squirrels, perhaps because of the stronger scent or a food preference, and this was the reward used for the remaining observations at this site.

The reward capsule was filled and glued to the bottom section, no more than 15 min before the trial began, as the squirrels appeared to lose interest in capsules filled more than 15 min before exposure, perhaps because of the loss of volatile odors. The *Puck.js* is also set up, connected, and placed inside the *eNut* shortly before the trial began.

A singular *eNut* was offered to the cage of squirrels usually between 11 A.M. and 4:30 P.M., though also at different times (ranging from 9 A.M. to 6:30 P.M.). The *eNut* was released to the squirrels in one of two locations: a food station (accessible through a small hatch) or placed on top of their large wooden nest box. The location was chosen based on the squirrels' activity levels: when highly active, it was placed at the food station; if squirrels were nesting, it was placed on top of their nest. All *eNut* interactions were observed and simultaneously recorded on video (smart phone). Accelerometer and gyroscope data recording began immediately when the squirrel picked up the *eNut*.

Fig. 5. Snapshots of a squirrel on the UC Berkeley campus interacting with an *eNut* prototype.

During the span of the experiment, we marked timestamps where the squirrels started or stopped a new behavior/activity, or when the squirrels moved to a new location. Most trials were completed in a single location but squirrels moved up to three times in some trials. Timestamps were also marked for *eNut* events, such as its successful opening or being dropped. A total of twenty experiments were conducted in this environment over the month of June 2023.

B. Rewilding Site 2: Captive Juvenile Eastern Gray Squirrels

1) Study Animals: The second site was located in Marin County, CA, and operated by a second wildlife rehabilitation organization. Five juvenile Eastern Gray Squirrels (8–10 weeks of age) were released into a large outdoor enclosure in May 2023. Their movements were recorded for two weeks starting in late May, and they were released into natural habitat in Marin County at the end of June.

2) Procedure: The outdoor cage was instrumented with the RFID gate readers and cameras. Its primary function for the present study was the validation of the RFID readers. This was done by using event recorder software (Noldus Observer XT) to identify the date and timestamp of movements and behaviors from video recordings. We then manually cross checked the timestamps to obtain the identity of squirrels passing the gate at different times, with the events recorded at the same time by the RFID reader.

C. Site 3: Free-Ranging Campus Adult Fox Squirrels

The third site was located in Berkeley, CA. Its primary function for the present study was the collection of baseline *eNut* manipulation data with experienced adult squirrels, as depicted in Fig. 5. Adult tree squirrels are highly habituated to humans on university campuses and we have studied the foraging and movement dynamics of campus squirrels on the UC Berkeley campus [23], [31]. The goal of the squirrel research is to understand the behavioral ecology of cognitive challenges faced by free-ranging wild animals. Scatter hoarding species, both squirrels and many species of birds, show highly sophisticated spatial abilities and decision-making processes, as well as brain specializations [27]. Studying cognition in the wild in

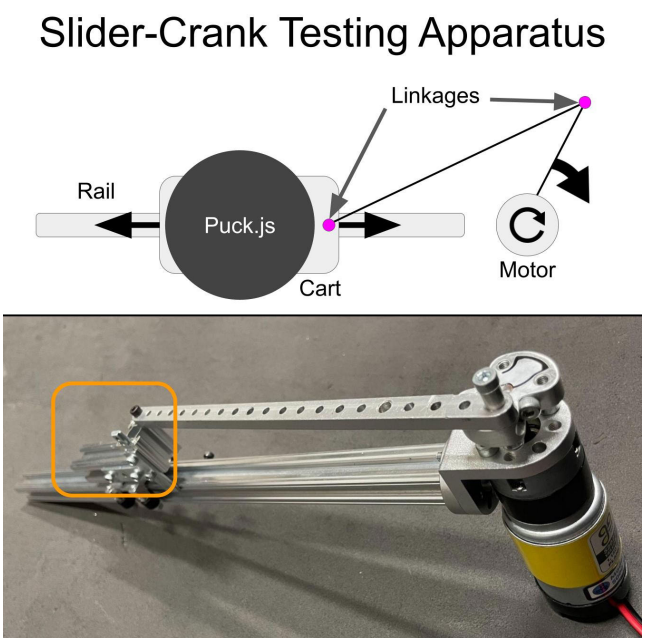

Fig. 6. Motor-driven slider-crank apparatus designed specifically for validating sensor data and methods for data analysis for this study. The diagram above is the top-down view of the apparatus, whereas the bottom image is the assembled apparatus. The *Puck.js* is mounted securely on the cart, highlighted in the orange box.

such champion species, both in terms of complex foraging and locomotory decisions [23], contextualizes the same processes studied in more generalist species, such as the domesticated laboratory rat [42], [43].

For this specific study, we used the mobile application data collection pipeline to collect data at Site 3; this method was flexible and convenient in this field context, where squirrel movements were unpredictable. The experiments were conducted over three separate days, with an average of 2–3 individual squirrels on each day.

D. Institutional Approval

This research was conducted under a protocol approved by the University of California at Berkeley Animal Care and Use Committee.

V. Validation Data for Data Processing

A. Accelerometer Data

1) Experiment 1: Slider Crank: Assessing the field work accuracy of data collected by the IMU required a testing apparatus. One such apparatus was created for the purpose of validating the *eNut*. This apparatus, depicted in Fig. 6, is a motor-driven slider-crank linkage with a cart acting as a piston constrained to 1-D motion on a rail. The cart is mounted to the rail with ball-bearing rollers and the *Puck.js* was securely mounted to the cart, such that only one of the accelerometer's axes aligned with the direction of motion. This linear motion profile mimics that of simple harmonic motion due to the nature of the crank revolving around the motor output shaft. By changing the motor output shaft speed, the oscillation frequency can be controlled.

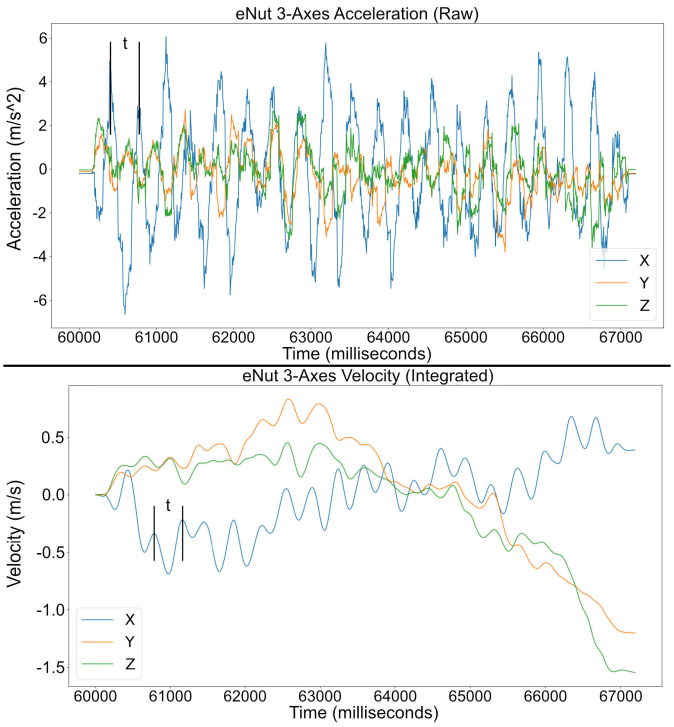

Fig. 7. **Top:** slider-crank oscillated raw accelerometer data in all three axes, showing instantaneous acceleration in m/s^2. **Bottom:** single-integrated accelerometer data from the slider-crank apparatus in all three axes, showing instantaneous velocities in m/s.

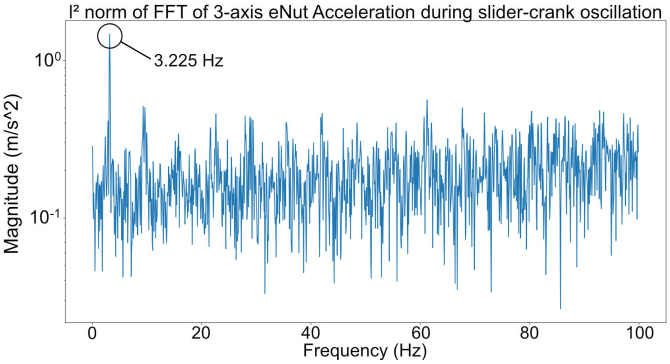

Fig. 8. l^2 norm of FFTs of each of the three accelerometer axes from the slider-crank oscillation data. The components of gravity resulted in an offset and peak in the FFT at 0 Hz, which is not shown.

However, the raw oscillation data itself included extraneous high-frequency noise due to the nonideal motion of the cart. A moving average filter removes this noise and produces the data, depicted in Fig. 7. We validated the real-world motion by double integrating the net instantaneous acceleration to calculate the position as a function of time. Fig. 7 shows the single-integrated accelerometer data for each axis, but there is a significant amount of drift, which only becomes worse in the double-integrated signal. This is likely due to the nature of the accelerometer sensor itself, and is compounded by error introduced by the the nonideal motion of the system. Theoretically, the motion should be similar to that of simple harmonic motion, but the reality is that this system produces imperfect sinusoidal motion, due to several variables, including frictions.

When applying the FFT on the raw accelerations in each axis and combining them, the visible peak (shown in Fig. 8)

is at 3.225 Hz which matches the expected frequency of approximately 3–4 Hz, as an 1150 RPM motor was running at 20% power. The combined FFTs of all three axes are computed as follows:[2]

$$\text{FFT}_{\text{combined}} = \sqrt{(\text{FFT}\,(a_x))^2 + \left(\text{FFT}\,\left(a_y\right)\right)^2 + (\text{FFT}\,(a_z))^2}. \tag{1}$$

This peak in the FFT is not significantly higher than the rest of the FFT signal, due to noise in the accelerometer signal. This figure shows that although the accelerometer data may be inherently noisy (and drift is likely when integrating across longer time series), the FFT of the accelerometer data is still useful for determining the amplitudes and frequencies of shaking in field work experiments.

2) Experiment 2: Hand Oscillation: Another form of data validation was oscillating the *Puck.js* approximately 10 cm back and forth by hand and recording data for two experiments, one each for the accelerometer's x- and y-axes. Although there is non-negligible human-introduced error in this motion, the experiment was still useful for analysis.

Fig. 9 shows the raw accelerations in all three axes for oscillation by hand in the y- and x-axes respectively. This method, even with a moving average filter, shows the inherent noise in the accelerometer readings, but can be used to extract metrics such as idle time and motion across the series by applying a certain threshold. The magnitudes displayed in the figures show a frequency of oscillation very similar to that of the experiment: six oscillations in 10 s, which matches the expected 0.6 Hz, also matching the FFT analysis shown later.

Figs. 10 and 11 show the single-integrated and double-integrated acceleration, in all three axes, for oscillations in the y- and x-axes respectively. To avoid accumulating error from the steady-state sensor bias, we estimate the dc offset and shift the signal so that it is centered around 0. This method is not completely immune to accumulation error across longer periods of time, but these experiments were short enough to show the prominent motion profiles in the second-integral graphs (position as a function of time) despite the error. The first graph in Fig. 10 shows the first integration of the originally noisy accelerometer signal, with oscillation in only one of the axes, as expected. However, in Fig. 11, there is a clear drift in the second integration of the accelerometer data due to inaccuracies in our method of removing the sensor noise and constant sensor offset in each axis.

As expected, the double-integrated graph shows sinusoidal oscillations with an approximate magnitude of 0.1 m. However, in both the x and y accelerometer oscillation experiments, a gradual drift is apparent, which can be reduced with higher sampling frequencies as well as high-speed on-device integration calculations, rather than integrating during the postprocessing stage.

Such controlled experiments to validate the accelerometer signal show the inherent noisiness in measured signals, which,

[2]The slight abuse of notation (intentional for simplicity) in this formula is to be understood as follows: $\text{FFT}_{\text{combined}}$ is a vector containing the magnitudes of FFT spectrum components, hence each of the $(\text{FFT}(a_i))^2$, $i = x, y, z$ is the vector of squared magnitudes of FFT spectrum components and $\text{FFT}_{\text{combined}}$ is a vector of same size.

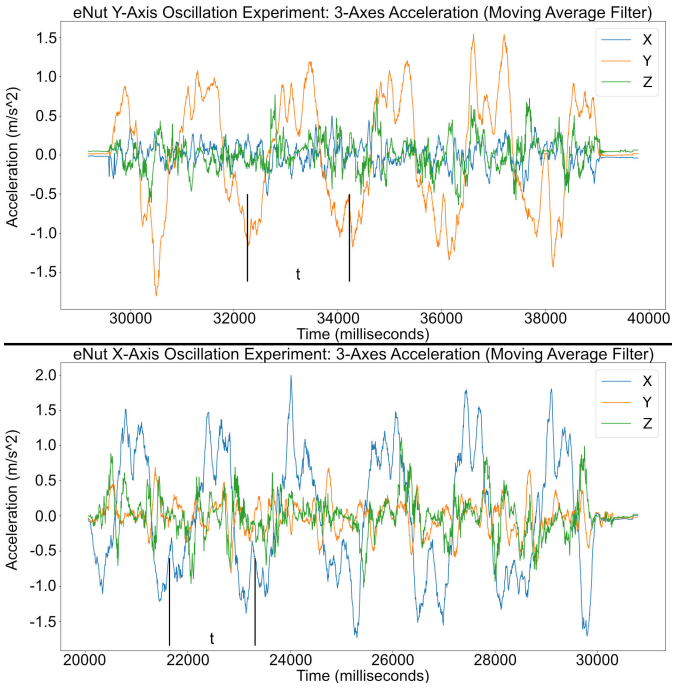

Fig. 9. Hand-oscillated y- and x-axis raw accelerometer data in all three axes, showing instantaneous acceleration in m/s^2 respectively.

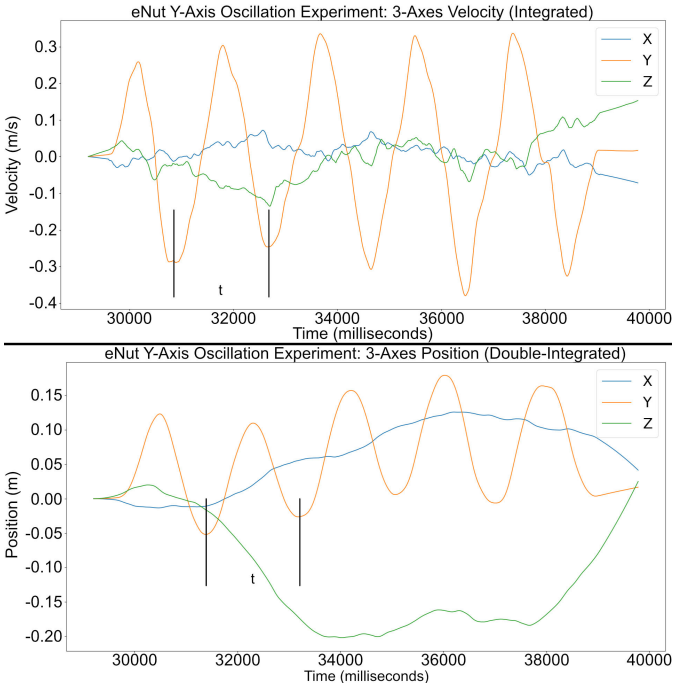

Fig. 10. Hand-oscillated y-axis single- and double-integrated (respectively) accelerometer data in all three axes, showing change in velocity (m/s) and change in position (m).

across longer time horizons, can cause accumulation inaccuracies, proving the accelerometer to be less useful in extracting accurate measurements. However, major axes of acceleration and/or oscillation can be extracted, as well as high-level trends of motion profiles.

Generally, accelerometer data is quite noisy, and tends to drift as well. In practice, estimating distance using an accelerometer over long periods of time can be inaccurate,

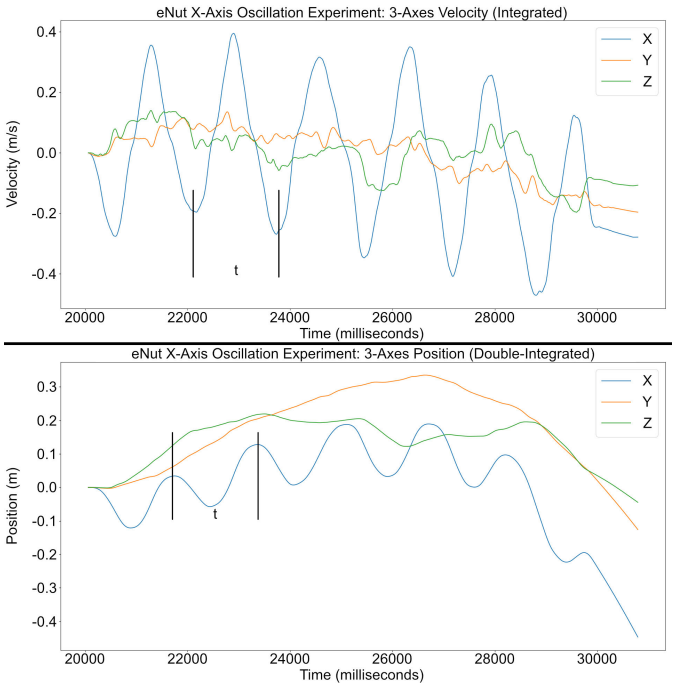

Fig. 11. Hand-oscillated x-axis single- and double-integrated (respectively) accelerometer data in all three axes, showing change in velocity (m/s) and change in position (m).

due to the random bias drift which gets doubly integrated over time [44]. Using signal processing techniques like Kalman filters can be effective in reducing random bias drift, but only for short-duration distance estimation [45]. Still, there are various challenges with the processing of IMU data for applications such as attitude estimation of moving vehicles, as accelerometers are not immune to external accelerations (e.g., those produced by centripetal motion) and double integrating the acceleration can quickly cause divergence in the predicted and actual positions in 3-D space [46].

3) Fourier Analysis: Through our analysis of the FFT of these two experiments, we have shown that our data processing pipeline can identify the prominent frequencies of acceleration in real-world data. The method utilized to combine FFTs from all three axes is the same as (1), described earlier in this section. Fig. 12 shows the FFT of the raw signal with prominent peaks around 0.62–0.72 Hz, which are consistent with the five to six oscillations done in about nine seconds (an expected frequency of 0.55–0.66 Hz). Fig. 13 depicts unfiltered data, so higher frequencies of noise are present, but these can be removed with a low-pass filter, such as a moving average (boxcar) filter. Regardless, the most prominent peak in the FFT of the accelerometer data corresponds to the frequency of oscillation by hand.

4) Net Acceleration Analysis: To classify whether the *eNut* is moving or at rest, we use the unfiltered magnitude of the net acceleration, which is computed as follows:

$$a_{\text{net}} = \sqrt{(a_x - \mu_x)^2 + (a_y - \mu_y)^2 + (a_z - \mu_z)^2} \quad (2)$$

where a_i is the raw acceleration measured along axis i and μ_i is the average acceleration along axis i over the entire time series. The net acceleration is used to classify different

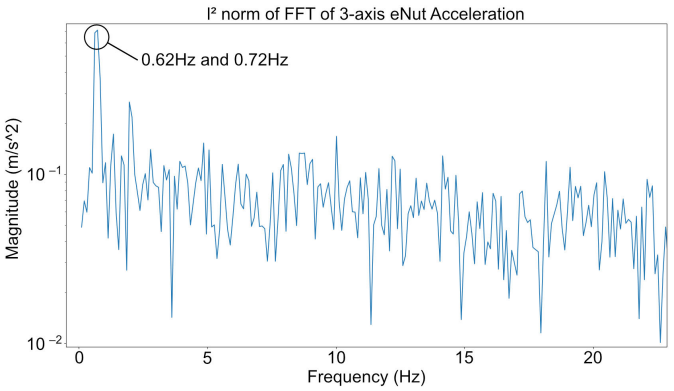

Fig. 12. FFT of the unfiltered net acceleration for one of the hand-oscillation experiments. The components of gravity resulted in an offset and peak in the FFT at 0 Hz, which is not shown.

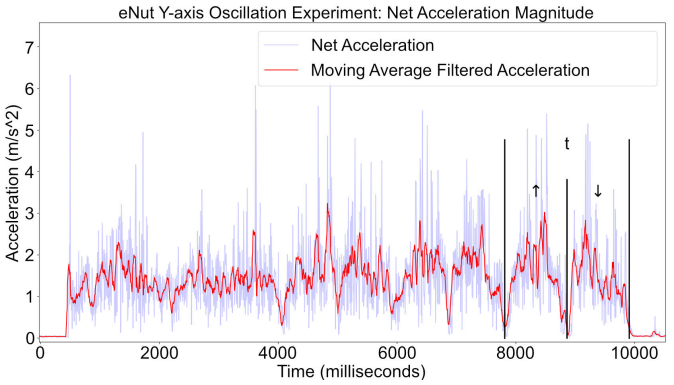

Fig. 13. Magnitude of net acceleration for oscillations in the y-axis, calculated by taking the l^2 norm of the acceleration in each of the three axes (unfiltered magnitude of acceleration in gray and moving-average filtered signal in red).

motion profiles and extract the total time spent for such. These include shaking time and idle time, which can both be seen visually in the net acceleration graph and classified programmatically by applying a threshold to a moving window of the net acceleration (i.e., if $a_{\text{net}} < a_{\text{threshold}}$: idle, else shaking).

B. Gyroscope Data

1) Experiment: Hand Oscillation: Validating the gyroscope data collection was done by oscillating the *Puck.js* between 0° and 180° by hand. Although there is non-negligible human-introduced error in this motion, the experiment was useful for analysis. Fig. 14 shows the raw gyroscope data in all three axes for oscillation by hand in the z-axis.

Fig. 14 shows the single-integrated angular velocities in all three axes to show the change in degrees with respect to time. To avoid accumulating from the steady-state sensor bias, we estimate the dc offset and shift the signal so that it is centered around 0. This method, as stated previously, is not completely immune to accumulation error across longer periods of time, but these experiments were short enough to show the motion profiles despite the error.

As expected, the graph of the integrated angular velocity shows the sinusoidal oscillation in the z-axis, with negligible accumulation in other axes. However, the graph shows that

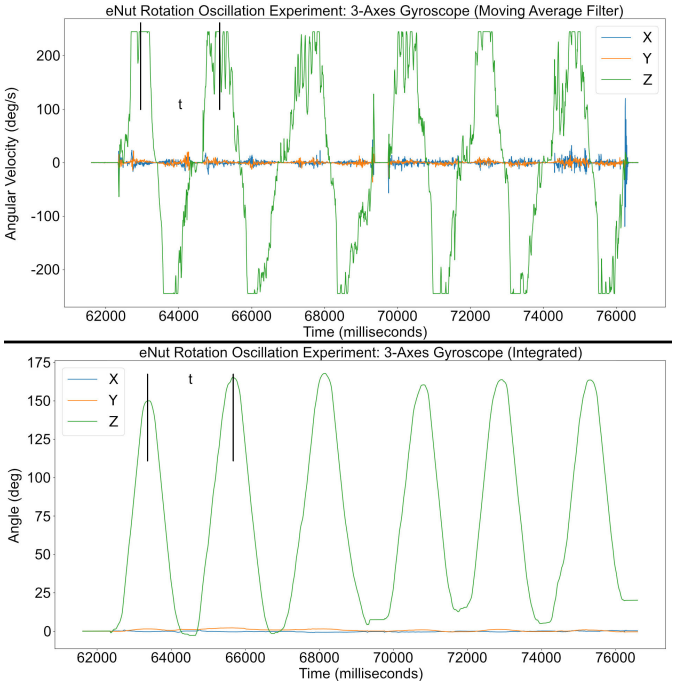

Fig. 14. **Top:** hand-oscillated raw gyroscope data in all three axes, showing instantaneous angular velocity in $^\circ/s$ (deg/s). **Bottom:** hand-oscillated z-axis single-integrated gyroscope data in all three axes, showing change in $^\circ$(deg).

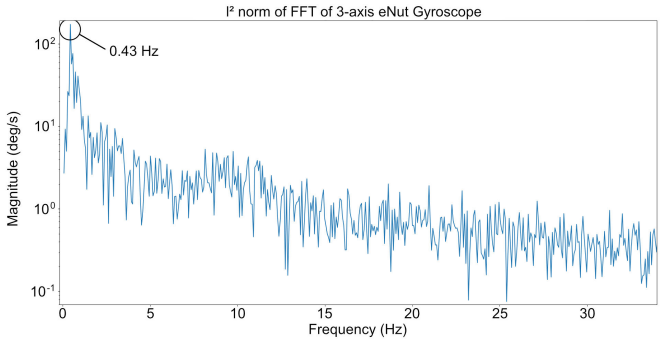

Fig. 15. FFT of unfiltered gyroscope data for hand-oscillation experiment. The dc offset resulted in a peak in the FFT at 0 Hz, which is not shown.

the amplitude of the oscillations ranges between 150° and 160°, but this error could be attributed to the gyroscope's limitations on the maximum angular velocity that can be measured. As shown in Fig. 14, the gyroscope cannot measure angular velocities above $245^\circ/s$, which is a known limitation of the sensor. The integrated gyroscope data is significantly less noisy than that of the accelerometer.

2) Fourier Analysis: Similar to the accelerometer data, the FFT of the gyroscope data allows us to validate its accuracy on controlled experiments before applying this technique to extract prominent frequencies of rotational motion from real-world data. The method utilized to combine FFTs from all three axes is the same as (1), described in Section V-A. Fig. 15 shows the FFT of the raw gyroscope signal with a prominent peak at approximately 0.43 Hz, which roughly corresponds to the six oscillations done in about 14 s (~ 0.428 Hz).

Similar to the raw and integrated signals, the FFT of the gyroscope data is less noisy than the accelerometer data,

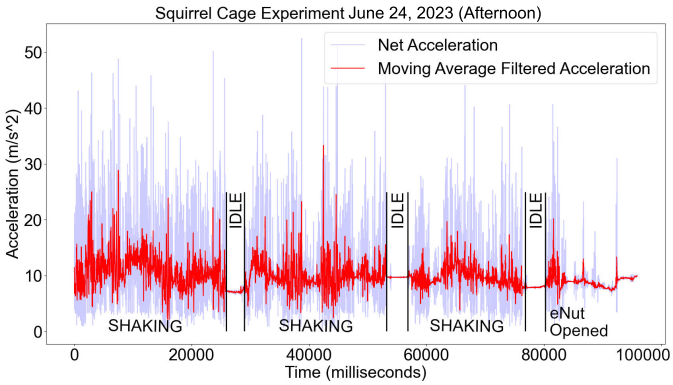

Fig. 16. Magnitude of net acceleration for a squirrel *eNut* opening experiment, calculated by taking the l^2 norm of the acceleration in each of the three axes (unfiltered magnitude of acceleration in gray and moving-average filtered signal in red).

and hence more useful for the analysis of rotational motion. Although the l^2 norm of $[\Delta\theta_x, \Delta\theta_y, \Delta\theta_z]^T$, where $\Delta\theta_i$ is the net rotation (integral of the angular velocity) in axis $i = x$, y, z, might not have a physical meaning that is easy to interpret, it is very likely that the animal, while grabbing the *eNut*, would apply the same periodicity of rotational motion in all three axes, due to muscular coupling (and with different magnitudes). This is because the axes of the applied rotational motion is likely to have nonzero components in the three axes dimensions simultaneously. Hence, taking the FFT of the l^2 norm of the integrated signal appeared to be a practical way to capture dominant frequencies visible in the full motion of the *eNut*, which was confirmed by the results.

VI. Preliminary Squirrel Data Collection

A. Accelerometer Data

By applying a threshold on the net acceleration during squirrel interactions with the *eNut*, we can separate the segments of the experiment in which the squirrel is shaking the *eNut* from those in which the *eNut* is idle. The method is the same as (2), described in Section V-A. Fig. 16 shows visually discernible sections of shaking and idle time, both of which correlate with the video analysis.

Applying the FFT (as described in Section V-A) on the entire recording of the squirrel opening the *eNut* results in irrelevant peaks, linked to frequencies of squirrel activity/engagement, as opposed to frequencies of motion. This is due to idle times. Idle times in the data also introduce lower (and higher, due to transients) frequencies in the decomposition. Hence, applying the FFT on a subset of the data is necessary to extract usable metrics on the frequencies of shaking. Fig. 17 shows an example of a specific subset of the data (which was selected by discerning time intervals of continuous shaking from the combined axes graph) from the same experiment as shown in Fig. 16.

Therefore, applying the FFT on a subset of the data, specifically on uninterrupted sections of shaking, provides the peak of interest: the frequency of shaking, as shown in Fig. 18. In this graph, there are significant peaks at 0.066 and 0.33 Hz, representing the frequencies of shaking during this subsection of the experiment. The 0.066 Hz frequency is due to the slow

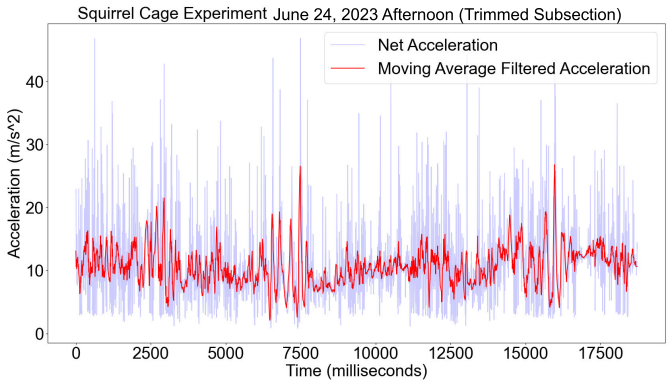

Fig. 17. Magnitude of net acceleration for a trimmed subsection of a squirrel *eNut* opening experiment, calculated by taking the l^2 norm of the acceleration in each of the three axes (unfiltered magnitude of acceleration in gray and moving-average filtered signal in red).

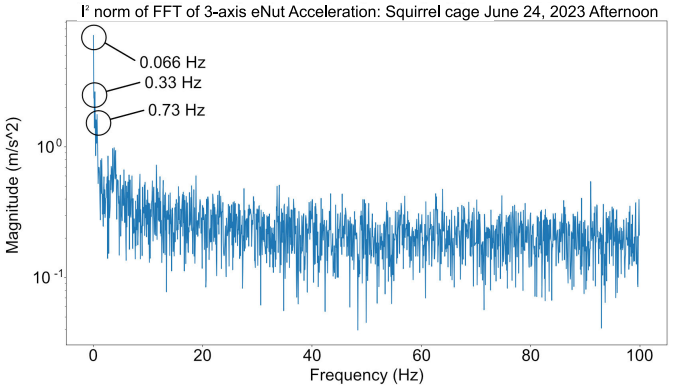

Fig. 18. FFT of a trimmed subset of all three axes of the unfiltered gyroscope data (combined through l^2 norm of axes) for the June 24, 2023 squirrel *eNut* opening experiment. The dc offset resulted in a peak in the FFT at 0 Hz, which is not shown. The highest nonzero peak is at 0.066 Hz.

rolling of the *eNut* and the 0.33 Hz is the quick rotation of the *eNut* as the squirrel gnaws on the screen. This was confirmed by the time-tagged video. The method utilized to combine FFTs from all three axes is the same as (1), described in Section V-A.

The raw accelerometer data in each axis, as shown in Fig. 19, is useful to understand primary axes of motion/shaking, but also can be used to calculate metrics such as maximum force applied (by multiplying the maximum instantaneous acceleration experienced by the sensor with the mass of the *eNut*: 39.03 g), as well as the average force/acceleration throughout the experiment or a specific subset of the signal. From the data in Fig. 19, we calculated that the maximum force in x-, y-, and z-axes are 0.61, 0.56, and 0.51 N respectively (given that the mass of the *eNut* is 39.03 g), and the average force applied throughout the entire experiment was approximately 0.56 N.

B. Gyroscope Data

Raw gyroscope signals, such as those depicted in Fig. 20, can be used to determine time intervals of idle and rotation time throughout the experiment. Based on video analysis of the squirrel experiments, the *eNut* was primarily experiencing rotational motions rather than shaking. Therefore, the

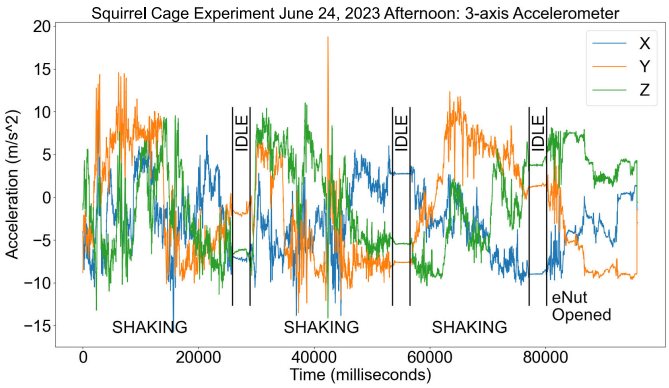

Fig. 19. Raw accelerometer data for all three axes from the June 24, 2023 squirrel *eNut* opening experiment.

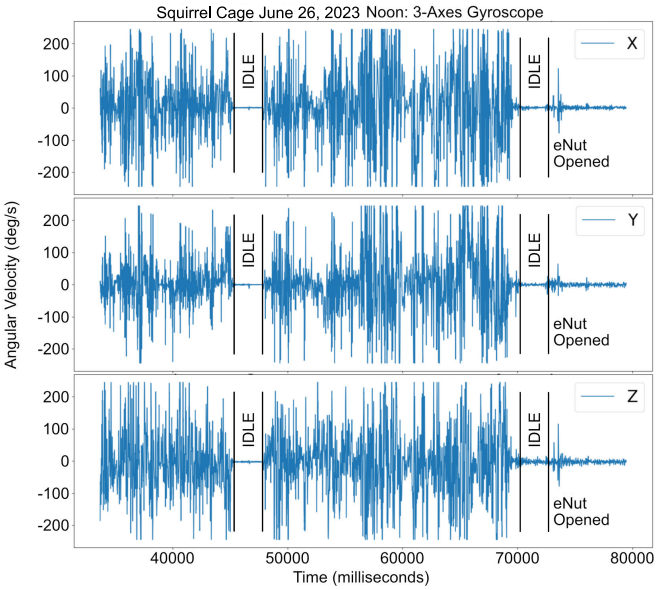

Fig. 20. Raw gyroscope signals for each of the three axes for the June 26, 2023 squirrel opening.

accelerometer signals presented above are likely projections of these rotational motions. Threshold analysis (as described in Section V-A4) is equally useful with the gyroscope signals. To classify events (shaking, idle, opening, etc.), we used the moving-average filtered data of all three gyroscope axes combined. The method utilized to combine all three axes of the gyroscope signals is as follows:

$$\omega_{\text{net}} = \sqrt{{\omega_x}^2 + {\omega_y}^2 + {\omega_z}^2} \tag{3}$$

where ω_x represent the angular velocity around the x-axis (and similar for y and z). It is thus expected that the spectral analysis of ω_{net} of (3) would reveal dominant peaks visible across the three axes of rotation. Fig. 21 showing the gyroscope signal for all axes combined has discernible features, such as idle periods between 12 000 and 15 000 ms and a sudden jolt at 40 000 ms, which correlate with the recorded video. This type of data extraction (event interval classification) is used to compare across experiments and determine trends in total idle times, opening time, and shaking times.

1) Analysis of Integrated Data: The integrated gyroscope signals are used to determine the total number of rotations in each axis as well as highlight events with major changes in the

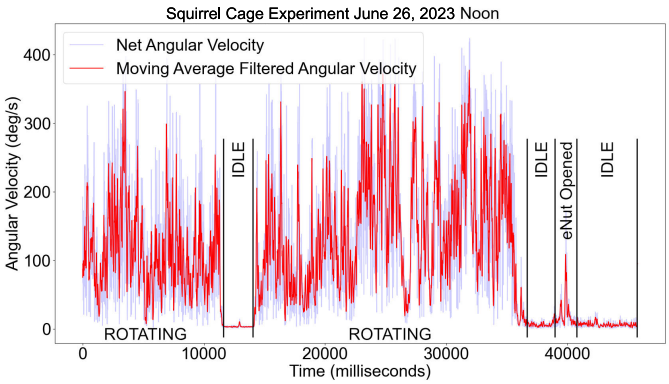

Fig. 21. Magnitude of net angular velocity for a squirrel *eNut* opening experiment, calculated by taking the l^2 norm of the angular velocity in each of the three axes (unfiltered magnitude of angular velocity in gray and moving-average filtered signal in red).

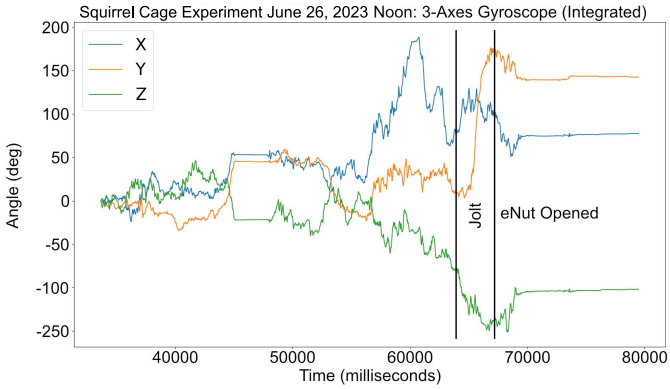

Fig. 22. Integrated signals for a successful *eNut* squirrel opening, depicting each axis integrated separately.

orientation of the *eNut* (e.g., if the *eNut* was suddenly flipped upside down). As shown in Fig. 22, the integrated gyroscope data shows certain moments when the squirrel rapidly rotates the *eNut*. The significant jump in orientation of the y-axis of the *eNut* near 65 000 ms in Fig. 22 directly correlates with the video, where the *eNut* was rotated upside down before being opened.

The integrated data from Fig. 22 can be compared to the integrated data of an unsuccessful opening, and across more trials, certain features that lead to successful openings can be extracted. For example, most successful openings appear to have a final jolt, which can be seen both in the raw gyroscope data as well as the integrated data. Fig. 23 shows the integrated gyroscope data for an unsuccessful opening, where a final jolt is not seen.

To compare trends in the total amount of rotation done by the squirrel between experiments, an integrated signal of the absolute value of the gyroscope signals for each axis can be graphed. Fig. 24 shows the cumulative rotation of the *eNut* across the entire June 26, 2023 Noon experiment. As shown, the *eNut* is rotated approximately 6.5 rotations in each of the axes before it was successfully opened. Displaying this metric across several experiments can provide insight into their ability to recognize the nut and make foraging decisions with it.

2) Fourier Analysis: The extracted subsections of the experiments' gyroscope data are also used for analyses of rotational frequencies by applying an FFT. This method of performing

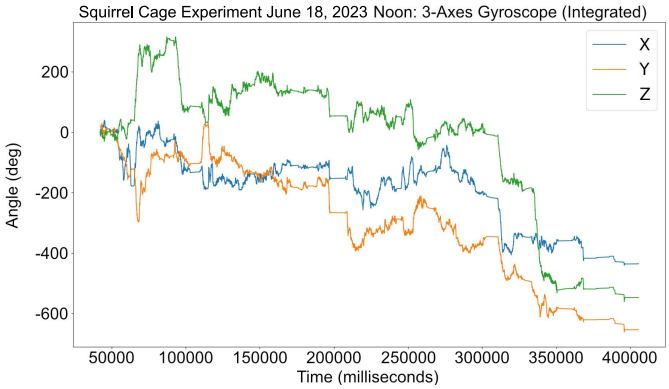

Fig. 23. Integrated signals for an unsuccessful *eNut* squirrel opening, depicting each axis integrated separately.

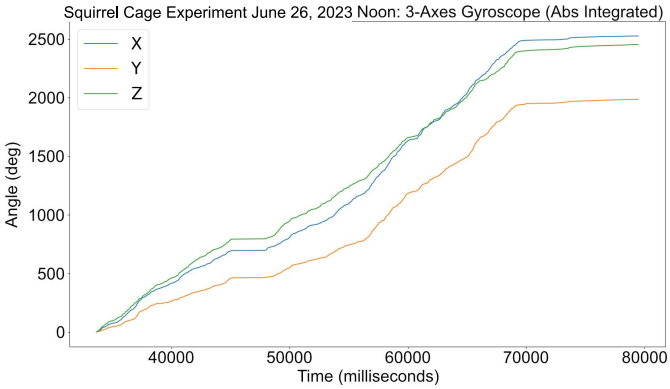

Fig. 24. Integrated absolute value of raw gyroscope angular velocity for each of the three axes from a trimmed subsection of the June 26, 2023 squirrel opening.

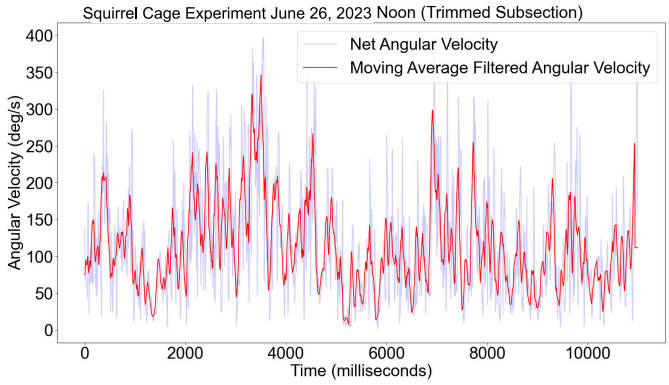

Fig. 25. Magnitude of net angular velocity for a trimmed subsection of a squirrel *eNut* opening experiment, calculated by taking the l^2 norm of the angular velocity in each of the three axes (unfiltered magnitude of angular velocity in gray and moving-average filtered signal in red).

FFTs on subsets of the experiment is more effective as idle time signals are not considered. The method to extract these subsets is similar to the one described previously: applying a threshold to a moving window of the net acceleration and comparing the average within the window if it is above the threshold (i.e., if $a_{\text{net}} < a_{\text{threshold}}$: idle, else shaking). Data segmentation can also be done by extracting signals based on time intervals of interest that are visually determined from the combined axes graphs. Fig. 25 shows a trimmed subset of the June 26, 2023 Noon squirrel opening.

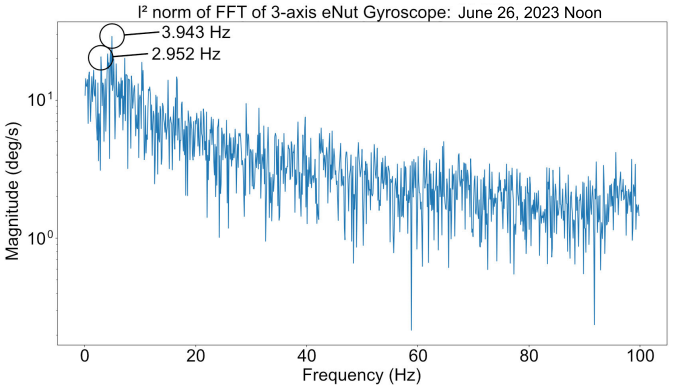

Fig. 26. FFT of a trimmed subset of all three axes of the unfiltered gyroscope data (combined through l^2 norm of axes) for the June 26, 2023 squirrel *eNut* opening experiment. The zero frequency peak was removed.

Applying an FFT on the trimmed data provides better insight on primary rotational frequencies for a section of the squirrel's interaction with the *eNut*. Fig. 26 depicts the FFT performed on a subset of the June 26, 2023 Noon squirrel opening, showing prominent peaks at 2.952 and 3.943 Hz, which are representative of the frequencies of angular velocities during this experiment. The method utilized to combine FFTs from all three axes is the same as (1), described in Section V-A.

C. RFID Gate Data

Our RFID monitoring system publishes live data on *ThingSpeak* (an IoT data analysis platform) as squirrels pass through the RFID gates. This data includes timestamps, the squirrel's unique identifier, and the specific gate they passed through. We also describe the setup of RFID gates and monitoring video cameras inside the Novato cage.

D. Video Data

In the Site 2 squirrel cage setup (Novato, CA), we had multiple monitoring video cameras mounted, which allowed us to record video data of squirrel behavior. We can access these recordings from the internal SD card in each camera, and then postprocess it to validate our sensing systems. This video data is manually analyzed using the Observer XT software from Noldus. Using this software, we are easily able to tag various behaviors seen in the video data, ranging from squirrels entering/exiting nest box, to squirrels rotating/shaking the *eNut*. Then, by comparing the events and their respective timestamps from the RFID logs and the video tags, we are able to validate the accuracy of our RFID gates. Our analysis of over 519 RFID gate crossings demonstrated that our RFID tag detection was above 98.1%, using video recordings as the ground truth. We calculated a 95% confidence interval to estimate the true accuracy of the RFID tag detection: (0.979612, 0.981792).

E. Summary of Derived Data

Using the *eNut* sensing system and custom data analysis software, we were then able to extract a variety of metrics, derived from the raw accelerometer and gyroscope time-series data.

1) Band of Actuation (in Frequency Domain): Using the FFT, we can identify the primary frequencies at which the squirrel rotates or shakes the *eNut*, and compare that to the maximum possible actuation frequency squirrels are capable of (e.g., when a squirrel scratches its ear).
2) Time Taken to Open the *eNut*: With the time-tags for each experiment, we can analyze the distribution of opening times in longitudinal studies to understand how squirrels learn on their own over multiple trials, and also by observing other squirrels' attempts to open the *eNut*.
3) Total Number of Rotations: By integrating the gyroscope data, we can determine how many times the squirrel rotated the *eNut*, which could also serve to quantify the amount of energy the squirrel spent in its attempt to open the *eNut*.
4) Distribution of Rotation Speeds (Including the Minimum, Maximum, and Average): We can generate histograms of the rotation speeds, and analyze the mean and variance of distributions over time, to understand the amount of energy the squirrel spends to open the *eNut*, and how it varies over time.
5) Distribution of Shaking Forces (Including the Minimum, Maximum, and Average): We can generate histograms of the shaking force (calculated from the acceleration data), and this would give us another way to quantify the amount of energy the squirrel spent to open the *eNut*, and how it varies over time.
6) Qualitative Data Extracted From Video: We can also classify the types of motion the squirrel performs, and compare that with whether they choose to open the *eNut* immediately or cache it for later (and also how far and how deep into the ground they end up caching the *eNut*, if at all).

These metrics can be used to quantify specific types of squirrel behavior and measure their learning (and analyze their decision-making processes) over long-term studies.

F. Datasets for Supervised Machine Learning Models

The multimodal data (combination of IMU, RFID, and video) collected by our system is especially useful because it provides us with labeled and annotated data that is essential for supervised machine learning applications. With such datasets, we can train models to identify squirrel behavior using only video data, which is generally challenging using traditional methods due to the scale and speed of their movements.

VII. Conclusion

A. Summary of Contributions

In this article, we presented the *eNut*, a three-part sensing system designed to monitor the activity of squirrels in the wild. The *eNut* itself is a custom 3-D printed walnut that contains an IMU embedded inside, which is paired with one of the three data collection pipelines we developed to receive and store the time-series sensor data. We also developed an RFID gate system to track squirrel behavior and uniquely identify the squirrel that is interacting with the *eNut*. Finally, we developed postprocessing data analysis tools to extract

various quantitative and qualitative metrics from the raw sensor data and video streams.

We then detailed the hardware setups we created for three different test sites for our initial round of experimentation with squirrels, and the metrics we extracted from real-world sensor data. We also confirmed the validity of our sensing system and the collected data using a custom test fixture, demonstrating that we can identify key parameters that describe the prescribed motion of the *eNut*, with a strong focus on the biological and psychological analyses of the quantitative and qualitative data collected with our system.

B. Potential Improvements

Our system currently allows us to record high-frequency accelerometer and gyroscope data from the *eNut*, at up to 250 Hz, and can detect squirrels passing through the RFID gates with over 98% accuracy. Although we have demonstrated the viability of combining both systems together with our Arduino data pipeline, system limitations prevent us from achieving the maximum possible data throughput in this pipeline. We proposed the future development of custom hardware that can support the highest data throughput for the *eNut* IMU data, while also maintaining the high reliability of RFID tag detection, without the use of software time-slicing.

The use of machine learning models to classify data can also aid in the extraction of valuable metrics, such as idle time, shaking time, and time to open the *eNut*. Several wearable devices use models such as support vector machines (SVMs) [47] and convolutional neural networks (CNNs) [48] to classify events, such as sitting, running, and eating. Such methods can assist in feature extraction, reducing the effort required for supervision and manual time-tagging of experiments. Although we do not have enough data to claim statistical significance of such trends measured, a larger dataset must be obtained—through methods outlined below—to statistically confirm whether most data presents similar trends. We outline a data collection system and have not run large-scale pilots, which would help in revealing statistical properties of the data, squirrel behavior, and interactions with the *eNut*.

C. Citizen Science Perspectives

In the future, our system can potentially be extended to enable large-scale citizen science studies all over the world. The *eNut* utilizes low-cost sensing hardware that can easily be configured and paired with our smartphone/laptop apps, which allows just about anyone to conduct field experiments with the squirrels in their vicinity. Potential next steps include the development of an open-source platform where anyone can document their experimental setup and upload their results. This would allow us to rapidly collect a wide range of data with different species of squirrels through crowdsourcing the collection process, in different environments, and with variations in the *eNut* size, shape, weight, and type of nut contained inside.

D. Future Psychology Research

Using the *eNut*, we plan to conduct future experiments in the three different test sites referenced earlier in order to gain a larger dataset for which proper analysis would be needed to be performed in order to confirm observed trends. We plan to introduce variations in the *eNut* size, shape, and weight, and study the correlation between the physical parameters and whether or not the squirrels immediately consume the nut or cache it for later.

Appendix

This section briefly illustrates the types of longitudinal data that can be collected from the work presented earlier, as well as the aggregate statistics that can be computed from it. With the time-tagging and collected data, the following examples show some of processed data that can be helpful for further animal studies.

1) Total Time for Each Opening: How long the squirrel spent trying to open each *eNut*; time-tagged video data can confirm the measurements collected from accelerometers and gyroscopes.
2) Evolution of the Opening Time Throughout the Duration of the Experiment: Fig. 27 illustrates the data collected through the experiment, and in particular a decreasing trend (using a linear regression model), showing learning of the squirrels, which become more proficient at *eNut* opening.
3) Activity Duration Distribution: Activity can be assessed by video, and categories include the following: opening, traveling, licking, rotation, shaking, and chewing—see Fig. 28.
    a) Average (or Cumulative) Opening Time: A combination of a chewing and rotating motion, where the squirrel attempts to pry open the *eNut* can be computed to assess the full duration of such processes (which involve cycling through different activities: chewing, rotating, etc.)—see the cumulative opening time is depicted as the sum of all the activity categories in Fig. 28.
    b) Idle Time: The squirrel is either just holding the *eNut* or has put it down, and is not moving or trying to open it in any way—refer to the dark blue section of Fig. 28.
    c) *eNut* Shaking Time: The squirrel is shaking the *eNut* with a back and forth motion for a duration that can be measured—illustrated in green in Fig. 28.
    d) *eNut* Chewing Time: The squirrel chews on the seam where the lid meets the body of the *eNut*; this is usually a prying motion, where the squirrels wedge their teeth between the two parts and attempt to pry them apart—illustrated in orange in Fig. 28.
    e) *eNut* Rotating Time: The squirrel rotates the *eNut* in a circular motion—illustrated in red in Fig. 28.
    f) *eNut* Licking Time: The squirrel sometimes licks the remaining peanut butter off of the top of the *eNut*—refer to the purple section of Fig. 28.
    g) Traveling Time: The time the squirrel spends traveling with the *eNut* can be measured; often, the squirrel moves around the cage with the *eNut*,

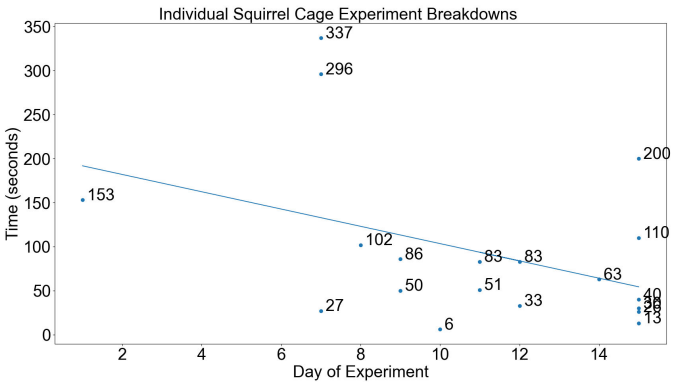

Fig. 27. Time evolution of the *eNut* opening time. Day one is the first opening on June 12th. The linear fit shows a downward trend, indicating that the squirrels learn and improve their *eNut* opening abilities throughout the duration of the experiment.

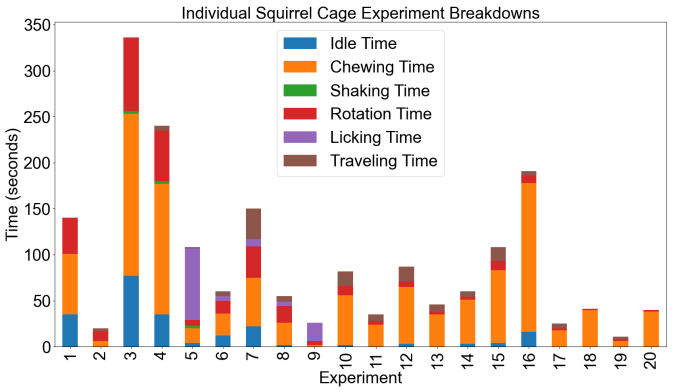

Fig. 28. Distribution of squirrel activity classification (by day and activity).

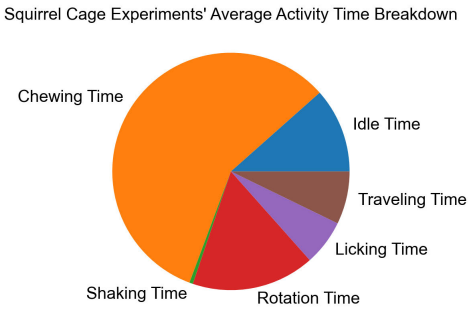

Fig. 29. Cumulative distribution of activity time exhibiting different behaviors throughout experiments.

going from one spot to another, usually running and jumping—illustrated in brown in Fig. 28.

4) Total Activity Time of Squirrels: Breakdown of activities throughout the entire experiment—refer to Fig. 29.

For this iteration of datasets and experimentation, the metrics were extracted manually using the time-tagged raw data, and correlated with video recordings of the experiments. In the future, this can be done automatically using custom-trained ML models, but doing so requires a significantly larger dataset from large-scale experiments in a variety of scenarios with a larger population of squirrels.

Fig. 30 depicts the net accelerometer and gyroscope plots, top and bottom respectively, that exhibit different types of

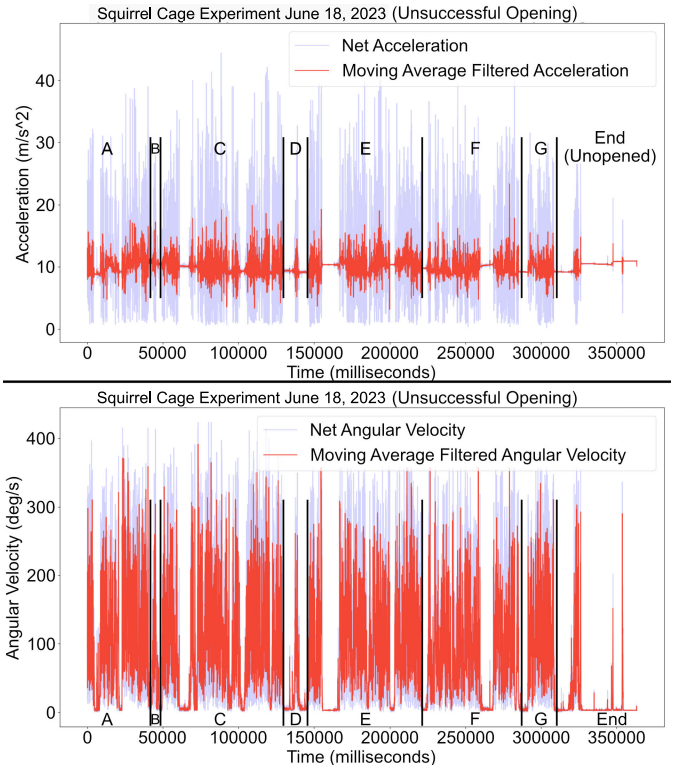

Fig. 30. Net accelerometer and gyroscope graphs generated from the squirrel cage experiment (unsuccessful) opening on June 18, 2023. Several methods of attempting to open the *eNut* were seen in the video analysis, which are denoted in both plots by lettered sections.

interactions with the *eNut*. This experiment was the one in which the squirrel did not succeed in opening the *eNut*, which allowed us to see a variety of opening techniques in the video analysis. Sections A, E, and F in Fig. 30 depict the squirrel rotating the *eNut* on its yaw axis, trying different angles at many spots along the glued seam. Section B shows the squirrel forcing the lid off at only one point with its incisors. In Section C, the squirrel rotates the *eNut* several times to find a different angle or possible opening to gnaw on. Sections D and G exhibit sudden shaking with the *eNut* held tightly in the squirrel's mouth.

ACKNOWLEDGMENT

The authors would like to thank the staff and volunteers of wildlife rescue organizations in Alameda County (Yggdrasil Urban Wildlife Rescue; yuwr.org) and Marin County (WildCare; discoverwildcare.org) for allowing them to observe juvenile squirrels in their facilities. WildCare staff Paula Holman, Lucy Burlingham, and Melanie Piazza and Yggdrasil director Lila Travis were generous and essential facilitators and collaborators for this study. The authors also want to thank Yggdrasil staff members Sylvie Mehner and Lara Klinkhammer for their invaluable assistance in setting up the study. They would also like to thank Berkeley undergraduates Marissa Grimes, for assistance in the observations, and Hriday Sheth, for his contribution toward the RFID readers. Finally, they would like to thank Yuliy Baryshnikov (University of Illinois Urbana-Champaign) for contributing the idea of instrumenting a squirrel's food item.

REFERENCES

[1] R. Wilson, E. Shepard, and N. Liebsch, "Prying into the intimate details of animal lives: Use of a daily diary on animals," *Endangered Species Res.*, vol. 4, pp. 123–137, Jan. 2008.

[2] D. Tuia et al., "Perspectives in machine learning for wildlife conservation," *Nature Commun.*, vol. 13, no. 1, p. 792, Jun. 2022.

[3] C. C. Wilmers, B. Nickel, C. M. Bryce, J. A. Smith, R. E. Wheat, and V. Yovovich, "The golden age of bio-logging: How animal-borne sensors are advancing the frontiers of ecology," *Ecology*, vol. 96, no. 7, pp. 1741–1753, Jul. 2015.

[4] H. Wang, A. O. Fapojuwo, and R. J. Davies, "A wireless sensor network for feedlot animal health monitoring," *IEEE Sensors J.*, vol. 16, no. 16, pp. 6433–6446, Aug. 2016.

[5] A. Kumar and G. P. Hancke, "A zigbee-based animal health monitoring system," *IEEE Sensors J.*, vol. 15, no. 1, pp. 610–617, Jan. 2015.

[6] D.-N. Tran, T. N. Nguyen, P. C. P. Khanh, and D.-T. Tran, "An IoT-based design using accelerometers in animal behavior recognition systems," *IEEE Sensors J.*, vol. 22, no. 18, pp. 17515–17528, Sep. 2022.

[7] A. Patel, B. Stocks, C. Fisher, F. Nicolls, and E. Boje, "Tracking the cheetah tail using animal-borne cameras, GPS, and an IMU," *IEEE Sensors Lett.*, vol. 1, no. 4, pp. 1–4, Aug. 2017.

[8] J. Ahn, J. Kwon, H. Nam, H.-K. Jang, and J.-I. Kim, "Pet buddy: A wearable device for canine behavior recognition using a single IMU," in *Proc. Int. Conf. Big Data Smart Comput.*, Jan. 2016, pp. 419–422.

[9] C. Rutz and G. C. Hays, "New frontiers in biologging science," *Biol. Lett.*, vol. 5, no. 3, pp. 289–292, Jun. 2009.

[10] R. Nathan, O. Spiegel, S. Fortmann-Roe, R. Harel, M. Wikelski, and W. M. Getz, "Using tri-axial acceleration data to identify behavioral modes of free-ranging animals: General concepts and tools illustrated for griffon vultures," *J. Experim. Biol.*, vol. 215, no. 6, pp. 986–996, Mar. 2012.

[11] J. J. Lahoz-Monfort and M. J. L. Magrath, "A comprehensive overview of technologies for species and habitat monitoring and conservation," *BioScience*, vol. 71, no. 10, pp. 1038–1062, Oct. 2021.

[12] G. Sántha and G. Hermann, "Accelerometer based activity monitoring system for behavioural analysis of free-roaming animals," in *Proc. IEEE 11th Int. Symp. Intell. Syst. Informat. (SISY)*, Sep. 2013, pp. 199–203.

[13] S.-L. Tan, N. Ha Duy, J. García-Guzmán, and F. García-Orduña, "A wireless activity monitoring system for monkey behavioural study," in *Proc. IEEE 15th Int. Symp. Consum. Electron. (ISCE)*, Jun. 2011, pp. 40–45.

[14] F. Höflinger et al., "Motion capture sensor to monitor movement patterns in animal models of disease," in *Proc. IEEE 6th Latin Amer. Symp. Circuits Syst. (LASCAS)*, Feb. 2015, pp. 1–4.

[15] A. N. Manikanta, A. F. Baba, D. S. Vyshnavi, D. K. Paul, and S. S. Sreedhar, "Cloud IoT based surveillance system for tracking and monitoring of domestic animals," in *Proc. Int. Conf. Integr. Circuits Commun. Syst. (ICICACS)*, Feb. 2024, pp. 1–5.

[16] P. Franč ek, K. Jambrosić, M. Horvat, and V. Planinec, "The performance of inertial measurement unit sensors on various hardware platforms for binaural head-tracking applications," *Sensors*, vol. 23, no. 2, p. 872, Jan. 2023.

[17] A. V. Rudyk, A. O. Semenov, N. Kryvinska, O. O. Semenova, V. P. Kvasnikov, and A. P. Safonyk, "Strapdown inertial navigation systems for positioning mobile robots—MEMS gyroscopes random errors analysis using Allan variance method," *Sensors*, vol. 20, no. 17, p. 4841, Aug. 2020.

[18] S. Bangera, T. Shiyana, G. Srinidhi, Y. Vasani, and S. Muligar, "MEMS-based IMU for pose estimation," in *Advances in Communication, Signal Processing, VLSI, and Embedded Systems*. 2020, pp. 1–14, doi: 10.1007/978-981-15-0626-0_1. [Online]. Available: https://www.researchgate.net/publication/337695213_MEMS-Based_IMU_for_Pose_Estimation

[19] A. K. Ross, J. C. Lawes, A. Elphinstone, S. Stutsel, and M. Letnic, "Headstarting as a cost-effective conservation strategy for an endangered mammal," *Current Biol.*, vol. 31, no. 10, pp. R465–R466, May 2021.

[20] J. G. Hendrix et al., "Territory acquisition mediates the influence of predators and climate on juvenile red squirrel survival," *J. Animal Ecol.*, vol. 89, no. 6, pp. 1408–1418, Jun. 2020.

[21] K. A. Sullivan, "Ontogeny of time budgets in Yellow-eyed juncos: Adaptation to ecological constaints," *Ecology*, vol. 69, no. 1, pp. 118–124, Feb. 1988.

[22] K. A. Sullivan, "Predation and starvation: Age-specific mortality in juvenile juncos (Junco phaenotus)," *J. Animal Ecology*, vol. 58, no. 1, p. 275, Feb. 1989.

[23] N. H. Hunt, J. Jinn, L. F. Jacobs, and R. J. Full, "Acrobatic squirrels learn to leap and land on tree branches without falling," *Science*, vol. 373, no. 6555, pp. 697–700, Aug. 2021.

[24] I. Eibl-Eibesfeldt, "Uber die ontogenetische entwicklung der technik des nusseoffnens vom eichhornchen," *Zeitschrift Fur Sugetierkunde*, vol. 21, pp. 132–134, Jun. 1956.

[25] N. Tamura, "Population differences and learning effects in walnut feeding technique by the Japanese squirrel," *J. Ethology*, vol. 29, no. 2, pp. 351–363, May 2011.

[26] P. D. Weigl and E. V. Hanson, "Observational learning and the feeding behavior of the red squirrel tamiasciurus hudsonicus: The ontogeny of optimization," *Ecology*, vol. 61, no. 2, pp. 213–218, Apr. 1980.

[27] A. N. Robin and L. F. Jacobs, "The socioeconomics of food hoarding in wild squirrels," *Current Opinion Behav. Sci.*, vol. 45, Jun. 2022, Art. no. 101139.

[28] L. F. Jacobs, "The effect of handling time on the decision to cache by grey squirrels," *Animal Behaviour*, vol. 43, no. 3, pp. 522–524, Mar. 1992.

[29] L. Z. Hadj-Chikh, M. A. Steele, and P. D. Smallwood, "Caching decisions by grey squirrels: A test of the handling time and perishability hypotheses," *Animal Behaviour*, vol. 52, no. 5, pp. 941–948, Nov. 1996.

[30] M. A. Steele and X. Yi, "Squirrel-seed interactions: The evolutionary strategies and impact of squirrels as both seed predators and seed dispersers," *Frontiers Ecology Evol.*, vol. 8, pp. 1–24, Aug. 2020.

[31] S. D. Preston and L. F. Jacobs, "Mechanisms of cache decision making in fox squirrels (sciurus niger)," *J. Mammalogy*, vol. 90, no. 4, pp. 787–795, Aug. 2009.

[32] M. M. Delgado, M. Nicholas, D. J. Petrie, and L. F. Jacobs, "Fox squirrels match food assessment and cache effort to value and scarcity," *PLoS One*, vol. 9, no. 3, Mar. 2014, Art. no. e92892.

[33] M. M. Delgado and L. F. Jacobs, "Caching for where and what: Evidence for a mnemonic strategy in a scatter-hoarder," *Roy. Soc. Open Sci.*, vol. 4, no. 9, Sep. 2017, Art. no. 170958.

[34] J. D. Ligon and D. J. Martin, "Piñon seed assessment by the piñon jay, gymnorhinus cyanocephalus," *Animal Behaviour*, vol. 22, no. 2, pp. 421–429, 1974.

[35] L. S. Johnson, J. M. Marzluff, and R. P. Balda, "Handling of pinyon pine seed by the Clark's nutcracker," *Condor*, vol. 89, no. 1, p. 117, Feb. 1987.

[36] P. G. Jablonski, S.-I. Lee, E. Fuszara, M. Fuszara, C. Jeong, and W. Y. Lee, "Proximate mechanisms of detecting nut properties in a wild population of Mexican jays (Aphelocoma ultramarina)," *J. Ornithology*, vol. 156, no. S1, pp. 163–172, Dec. 2015.

[37] S. B. V. Wall, "The evolutionary ecology of nut dispersal," *Botanical Rev.*, vol. 67, no. 1, pp. 74–117, Jan. 2001.

[38] G. L. Xiong et al., "Real-time video detection of falls in dementia care facility and reduced emergency care," *Amer. J. Managed Care*, vol. 25, pp. 314–315, 2019.

[39] B. Zylstra et al., "Extended, continuous measures of functional status in community dwelling persons with Alzheimer's and related dementia: Infrastructure, performance, tradeoffs, preliminary data, and promise," *J. Neurosci. Methods*, vol. 300, pp. 59–67, Apr. 2018.

[40] *Arduino Forum Post: FDX-B 134.2 KHz RFID Reader*. Accessed: Jun. 2022. [Online]. Available: https://forum.arduino.cc/t/fdx-b-134-2-khz-rfid-reader/912859/18

[41] E. S. Bridge et al., "An arduino-based RFID platform for animal research," *Frontiers Ecology Evol.*, vol. 7, pp. 1–20, Jul. 2019.

[42] D. F. Sherry, L. F. Jacobs, and S. J. C. Gaulin, "The hippocampus and spatial memory: Reply," *Trends Neurosciences*, vol. 16, no. 2, p. 57, 1993.

[43] H. L. Payne, G. F. Lynch, and D. Aronov, "Neural representations of space in the hippocampus of a food-caching bird," *Science*, vol. 373, no. 6552, pp. 343–348, Jul. 2021.

[44] G. Pang and H. Liu, "Evaluation of a low-cost MEMS accelerometer for distance measurement," *J. Intell. Robotic Syst.*, vol. 30, no. 3, pp. 249–265, 2001.

[45] H. H. S. Liu and G. K. H. Pang, "Accelerometer for mobile robot positioning," *IEEE Trans. Ind. Appl.*, vol. 37, no. 3, pp. 812–819, 2001.

[46] H. Ahmed and M. Tahir, "Accurate attitude estimation of a moving land vehicle using low-cost MEMS IMU sensors," *IEEE Trans. Intell. Transp. Syst.*, vol. 18, no. 7, pp. 1723–1739, Jul. 2017.

[47] X. Zhan, Q. Huang, C. Zhu, X. Li, and G. Liu, "A real-time police dog action recognition system based on vision and IMU sensors," in *Proc. IEEE Int. Conf. Multimedia Expo. Workshops (ICMEW)*, Jul. 2020, pp. 1–2.

[48] Z. Pan, H. Chen, W. Zhong, A. Wang, and C. Zheng, "A CNN-based animal behavior recognition algorithm for wearable devices," *IEEE Sensors J.*, vol. 23, no. 5, pp. 5156–5164, Mar. 2023.

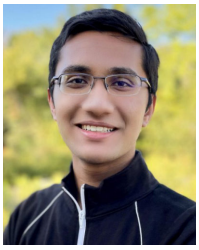

Mihir S. Chauhan is pursuing the B.S. degree in computer science with Purdue University, West Lafayette, IN, USA.

He is a Research Intern with the Electrical Engineering and Computer Sciences Department, University of California at Berkeley, Berkeley, CA, USA. He is also the Co-Founder and a Lead Developer of a robotics simulation and learning platform used by over 40 000 users worldwide. He has a background in robotics, as the team captain of a competitive robotics team. His work on a portable water harvesting machine was showcased at the Smithsonian Museum's Futures exhibition.

Mr. Chauhan has won several international recognitions, such as the Dean's List Finalist and the Two-Time Finalist at the World Championship.

Avikam Chauhan (Member, IEEE) received the B.A. degree in computer science and the M.S. degree in electrical engineering and computer sciences from the University of California at Berkeley, Berkeley, CA, USA, in 2023 and 2024, respectively.

From 2022 to 2024, he was a Student Researcher with Berkeley Artificial Intelligence Research Laboratory, with a focus on machine learning for connected autonomous vehicles. He is currently a Software Engineer with Applied Intuition, Mountain View, CA, USA, working on cutting-edge machine learning research and development for autonomous vehicle software.

Mr. Chauhan received the Dwight D. Eisenhower Transportation Fellowship from the United States Department of Transportation for his research on Transformer-based vehicle behavior prediction models and large-scale GPU-parallelized traffic resimulation.

Myriam Bayen is a Sophomore with the Head Royce School, specializing in computer science. She is a Visiting Student with the Jacobs Lab of Cognitive Biology, UC Berkeley, Berkeley, CA, USA. She was an Intern with the Physical Medicine and Rehabilitation Departments, Sorbonne University Medical School (Hôpital Pitié Salpêtriére, Paris, France), in 2023. She is the President of the Head Royce Computer Science Club and the Girls X Math Club.

Ms. Bayen was selected as a Member of the IEEE ITTS Incubator Program at Cornell University in 2024. She was a recipient of the AP Scholar with Honor Award and the US President's Volunteer Service Award in 2024.

Fangyu Wu received the B.S. and M.S. degrees in civil and environmental engineering from the University of Illinois at Urbana–Champaign, Urbana, IL, USA, in 2016 and 2018, respectively, the M.Eng. degree in EECS from University of California at Berkeley (UC Berkeley), Berkeley, CA, USA, in 2019, and the Ph.D. degree from the Electrical Engineering and Computer Sciences Department, UC Berkeley, in 2024.

He is a Postdoctoral Researcher with Cornell University, Ithaca, NY, USA. His research interests encompass optimization approaches to multiagent robotic systems, with a focus on planning and control of automated vehicles.

Fahd A. Althukair received the B.S. degree in electrical engineering and computer sciences from the University of California at Berkeley, Berkeley, CA, USA, in 2023.

He is currently a Network Engineer with Aramco, Dhahran, Saudi Arabia, where he previously worked as a Full-Stack Developer developing network monitoring and automation tools.

Mr. Althukair was a recipient of the Scholarship from Saudi Aramco.

Michael T. Kaiser received the B.S. degree in environmental science from the University of Wisconsin-Madison, Madison, WI, USA, in 2014.

He is currently a Research Assistant with the Jacobs Lab of Cognitive Biology, University of California at Berkeley, Berkeley, CA, USA. Previously, he managed a research site in Sierra Leone, West Africa, in collaboration with the Max Planck Institute of Evolutionary Anthropology, Leipzig, Germany, where he investigated the ecological drivers of chimpanzee behavioral diversity. His current research interests include understanding the evolutionary pressures that shape the various sensory mechanisms mammals employ to interpret their environments.

Lucia F. Jacobs received the bachelors of science in biology (neuroscience and behavior) from Cornell University, Ithaca, NY, USA, in 1978, and the M.S. and Ph.D. degrees in ecology and evolution from Princeton University, Princeton, NJ, USA, in 1983 and 1987, respectively.

She is currently a Professor Emerita with the Department of Psychology and the Helen Wills Neuroscience Institute, University of California at Berkeley, Berkeley, CA, USA. She has authored more than 50 articles in peer-reviewed journals and conferences, integrating ecology, animal cognition, and neuroscience to study adaptive patterns of brain and behavior in diverse species.

Dr. Jacobs has received awards and honors that include Prytanean and Hellman Faculty Awards (University of California at Berkeley), a Herbert Spencer Lecture (University of Oxford), and the Radcliffe Fellowship (Radcliffe Institute for Advanced Study, Harvard University).